Corrosion Science 50 (2008) 3534–3541

Contents lists available at ScienceDirect

Corrosion Science

journal homepage: www.elsevier.com/locate/corsci

Effect of microstructure on the sulphide stress cracking susceptibility of a high strength pipeline steel

E. Ramírez [a], J.G. González-Rodriguez [a,*], A. Torres-Islas [a], S. Serna [a], B. Campillo [b], G. Dominguez-Patiño [a], J.A. Juárez-Islas [c]

[a] Centro de Investigación en Ingeniería y Ciencias Aplicadas-UAEM, Av. Universidad 1001, 62209-Cuernavaca, Mor., Mexico
[b] Intituto de Ciencias Físicas-Facultad de Químicas-Universidad Nacional Autónoma de México Cuernavaca, Mor., Mexico
[c] Instituto de Investigaciones en Materiales-Universidad Nacional Autónoma de México, Circuito Exterior S/N, Cd. Universitaria, C.P. 04510, Mexico, D.F., Mexico

ARTICLE INFO

Article history:
Received 24 June 2008
Accepted 13 September 2008
Available online 21 September 2008

Keywords:
A. Microalloyed steel
C. Hydrogen embrittlement
C. Sulphide stress cracking
Steel microstructure

ABSTRACT

The sulphide stress cracking (SSC) susceptibility of a newly developed high strength microalloyed steel with three different microstructures has been evaluated using the slow strain rate testing (SSRT) technique. Studies were complemented with potentiodynamic polarization curves and hydrogen permeation measurements. Material included a C–Mn steel having Ni, Cu, and Mo as main microalloying elements with three microstructures: martensitic, ferritic and ferritic + bainitic. Testing temperatures included 25, 50, 70 and 90 °C. Detailed SEM observations of the microstructure and fracture surfaces were done to identify possible degradation mechanisms. The results showed that in all cases, the corrosion rate, number of hydrogen atoms at the surface and the percentage reduction in area increased with temperature. The steel with a martensitic microstructure had the highest SSC susceptibility at all temperatures, whereas the ferritic steels were susceptible only at 25 °C, and the most likely mechanism is hydrogen embrittlement assisted by anodic dissolution.

1. Introduction

The oil industry contains a wide variety of corrosive environments. Mexican crude oil and gas commonly contain entrained water, CO_2 and H_2S. The transport of these type of products always induces failures in the pipeline systems, and not less frequently in the weld beads. Each year, tens of million of dollars are expended to replace or repair pipes and vessels that suffer excessive localized metal loss, stress corrosion cracking (SCC) or hydrogen embrittlement (HE). When sulphide is present, this type of brittle failure is known as sulphide stress cracking (SSC) [1], and it has been established as a particular case of HE. Hydrogen embrittlement can restrict the use of metals and alloys in aqueous environments. The degradation of mechanical properties as a result of hydrogen ingress is of particular concern in high strength alloys. Hydrogen concentration gradient, temperature, and locations with high hydrostatic stress [2] are responsible for hydrogen transport through steels. However, steel resistance to hydrogen embrittlement is largely affected by hydrogen concentration in trapping sites contained by their microstructure [3–5] and a big amount of research has been done on this matter [6–13].

High strength low alloy (HSLA) steels contain vanadium, niobium, and/or titanium. These elements are referred to as microalloying elements because only small amounts of them are required, and the steels are called microalloyed steels. These are very popular high strength steels that are used in a vast number of applications, including automobile frames, gas transmission pipelines, ship plate, bridge beams, and electrical power transmission poles. Microalloyed pipeline steels are extensively used in the oil and gas industry having severe mechanical requirements for sour service applications and deep water gas wells. Currently, grade steels higher than conventional X-52 have received a considerably interest. For their mechanical properties accomplishment, it has been recognized that technologies for steelmaking, plate rolling and pipe manufacturing have to be improved [14–16].

On the other hand, thermo mechanical processes such as controlled rolling of steel slabs provides quite a few advantages over normally rolled steels. For instance, it could produce steel plates with better strength, toughness and weldability combinations [17]. Improvement of these properties is due to different strengthening mechanism such as grain refinement; here simultaneously the enhancement of strength and toughness is feasible [18]. This mechanism is achievable by the precise control of the temperature during final rolling passes, combined with previously suitable chemical composition design and judiciously addition of microalloying elements to steel slab. In addition to recrystallization and transformation process during controlled rolling, final cooling procedures just after the last finish hot rolling pass can produce a variety of final steels microstructures. The transfer time from final rolling to differ-

* Corresponding author. Tel./fax: +52 777 3 29 70 84.
E-mail address: ggonzalez@uaem.mx (J.G. González-Rodriguez).

0010-938X/$ - see front matter © 2008 Elsevier Ltd. All rights reserved.
doi:10.1016/j.corsci.2008.09.014

ent cooling rates and starting cooling temperatures give us the ability to obtain the required yield strength and toughness [19–21] of contemporary pipelines required by oil and gas industry.

Nevertheless, to make possible the creation of reliable higher grades of pipes for sour environment service, hydrogen permeability evaluations as well as stress corrosion cracking tests have to be carried out. Furthermore, to ensure pipeline steels performance, identification of sour degradation mechanisms (i.e. hydrogen embrittlement) as a function of microstructure has to be done as well. Thus, the aim of this work is to evaluate the SSC susceptibility of a newly developed Fe–C–Mn controlled hot rolling steel with several final cooling media treatments, in order to evaluate its application as a pipeline steel.

2. Experimental procedure

2.1. Material

The chemical composition (in wt%) of microalloyed steel used was 0.044-C, 0.271-Si, 1.69-Mn, 0.0091-P, 0.0103-Cr, 0.240-Ni, 0.0010-V, 0.014-Ti, 0.2170-Cu, 0.25-Mo, 0.0310-Al, 0.0001-B, 0.0554-Nb, 0.0070-Sn, 0.055-As, 0.0018-Pb, 0.0037-Sb, 0.0016-Ca, 0.0040-N_2 and balance Fe. Slab samples were heated at 1250 °C, increasing the temperature from room temperature at a rate of 0.4 °C/s, soaked for 90 min and immediately hot rolled. Initially slab rough rolling was done in five passes within 1250–1098 °C range. Then, the rough rolling was followed by a cooling period until an experimental initial temperature for the final rolling procedure of 1051 °C was reached. This temperature was set according to the solubility of niobium carbonitride precipitation in austenite as reported elsewhere [15]. For steel composition the precipitation dissolution temperature was of 1067 °C. A finishing total deformation of 37% was achieved also in five passes ending at 867 °C. After the last final rolling pass, steel plates were cooled in forced nitrogen gas, sprayed water or water quench. The second and third cooling procedures were performed from 867 to 650 °C and then the plates were let to cool in air to room temperature, as summarized on Table 1. Thin foil specimens were prepared by a standard jet-polisher, and then examined with a JEOL-2000 EX transmission electron microscope (TEM).

2.2. SSRT tests and polarization curves

Cylindrical tensile specimens with a 25.00 mm gauge length and 2.50 mm gauge diameter were machined. Before testing, the specimens were abraded longitudinally with 600 grade emery paper, degreased, and masked, with the exception of the gauge length. Specimens were subjected to conventional, monotonic slow strain rate tensile (SSRT) testing in air as an inert environment, and in the standard NACE solution which consisted of 5% NaCl, with H_2S produced by reacting sodium sulfide (Na_2S) with acetic acid. This solution was deaerated with nitrogen gas at a strain rate of 1.00×10^{-6} s^{-1} at 25, 50, 75 and 90 °C. Temperature was controlled with a heating mantle with an error of ±3 °C All the tests were done at the open circuit potential. The loss in ductility was assessed in terms of the percentage reduction in area (%R.A) by using

$$\%\text{R.A.} = \frac{A_i - A_f}{A_i} \times 100 \quad (1)$$

where A_i and A_f are the initial and final area respectively. Tensile-fractured specimens were examined by a JEOL scanning electron microscope (SEM).

Potentiodynamic polarization curves were performed at a sweep rate of 1 mV/s using a fully automated AC Gill potentiostat controlled with a desk top computer in the NACE solution and test temperatures. For these tests, a saturated calomel reference electrode (SCE) and a graphite auxiliary electrode were used. Polarization curves were performed once the free corrosion potential value (E_{corr}) was stable, i.e. it did not change in a 2 mV/min range. Corrosion current values, I_{corr}, were calculated by using Tafel extrapolation method. For comparison, some tests were performed on a typical pipeline steel such as an X-60 type microalloyed steel.

2.3. Hydrogen permeation tests

The two cell component electrochemical permeation technique originally developed by Devanathan and Stachurski [22] was employed to determine the hydrogen permeation through steel membranes, with thickness about 0.7 mm and an effective exposed area of 1.00 cm^2. The surface finish was the same as that given to the specimens used for the polarization curves and the SSRT tests, i.e. abraded with 600 grade emery paper, washed and degreased with acetone. One of the faces of the membrane was Pd coated. The hydrogen exit (collection) compartment side contains an electrolyte which consisted of 0.5 M sodium hydroxide (NaOH) solution purged with nitrogen (N_2) gas. The specimen surface without Pd was exposed to this solution was potentiostatically passivated at a constant potential of +300 mV vs. SCE. A graphite rod was used as the auxiliary electrode. When the passive current reached a constant value, then the H_2S-containing (NACE) solution was poured into the hydrogen entry compartment, the Pd-coated specimen side, to start the hydrogen permeation experiments. Temperature was kept constant by using a heating tape at 25, 50, 70 and 90 °C. Once a steady state current permeation current density was observed at each temperature, the temperature was increased.

The resulting current gave a direct measure of the hydrogen flow rate, and the permeation transient was recorded throughout the experiment. Assuming that the overall hydrogen transport process is controlled by diffusion through the bulk material, transport will not be affected by reactions occurring on the membrane surface. For this study, the hydrogen flux (J_∞, mole H s^{-1} m^{-2}) through the specimen was measured in terms of current density $i_{\infty p}$, and converted to hydrogen flux according to the following equation:

$$J_\infty = \frac{i_p^\infty}{nF} \quad (2)$$

where n is the number of electrons transferred, F is Faraday's constant.

The effective hydrogen diffusivity D_{eff} (m^2/s), the diffusion of hydrogen through the material by taking trapping and obstacles into consideration, is calculated from the permeation transient curve using the well-known "time lag" method

$$D_{eff} = \frac{L^2}{6t_L} \quad (3)$$

Table 1
Heat treatment and mechanical properties of specimens under study

Specimen designation	Heat treatment	YS (MPa)	UTS (MPa)
2F	Water quenched from 867 °C	600	711
2A	Cooled from 867 to 600 °C with forced nitrogen gas and then cooled to room temperature	552	738
1T	Cooled from 867 to 600 °C sprayed water and then cooled to room temperature	498	638

where t_L is the lag time which is simply defined as 0.63 times the steady state value and L the specimen thickness. The number of hydrogen atoms at the entrance surface, C_0, the Pd coated, was calculated by using

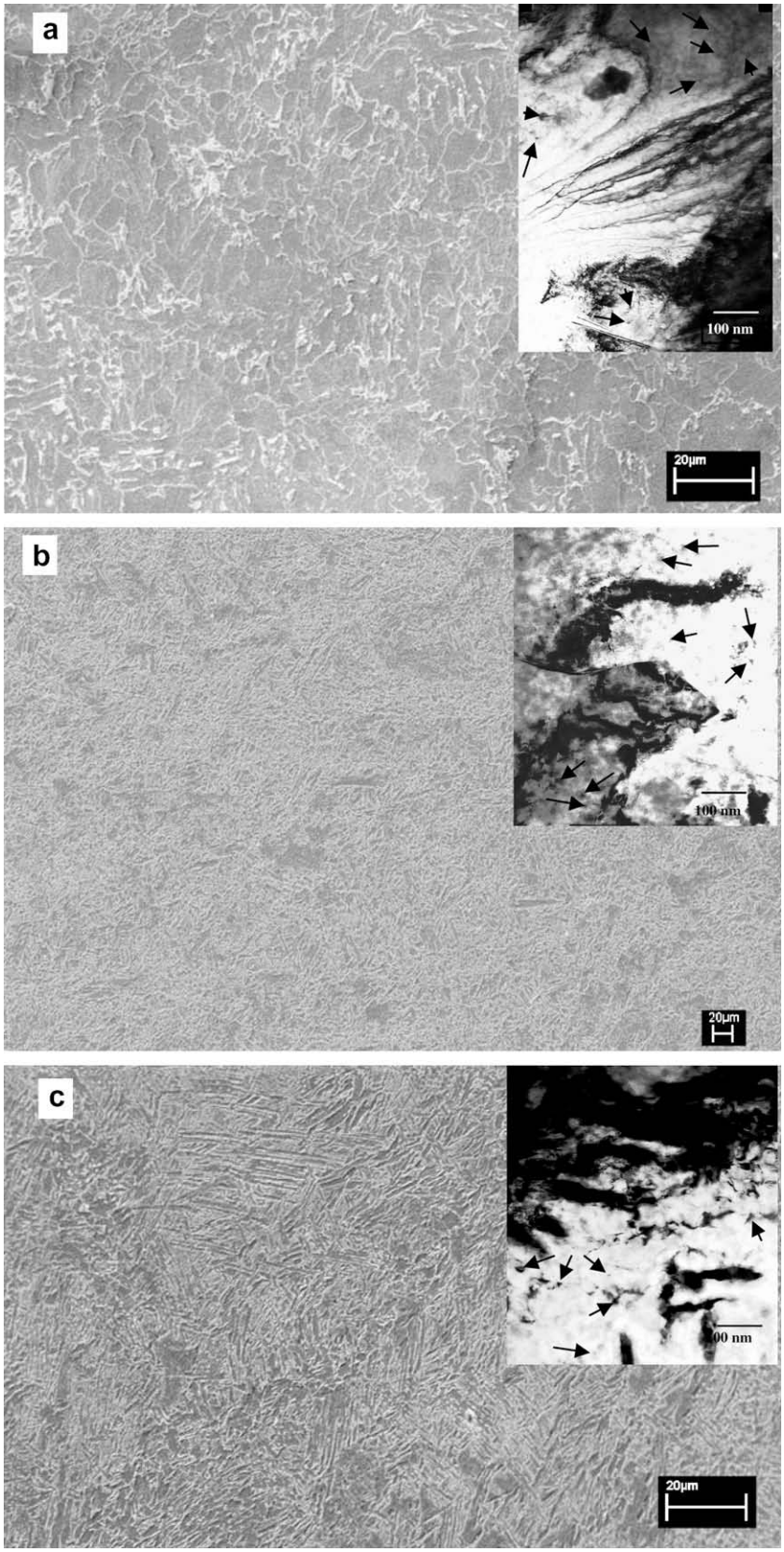

Fig. 1. Microstructures of steel: (a) 2A, (b) 1T and (c) 2F.

$$C_0 = \frac{J_\infty L}{D_{\text{eff}}} \quad (4)$$

3. Results and discussion

3.1. Steels microstructure and mechanical properties

Fig. 1 shows the resulting steels microstructures for the different cooling conditions. The microstructure of the forced nitrogen gas steel is shown in Fig. 1a, which consisted mainly of ferrite grains with an average grain size of 20–30 μm. In the same figure there are some bainite patches which grow from ferrite grains, and sub-grain boundaries. It has been reported elsewhere [15] the presence of small precipitates with a size of ~20 nm (see insert on Fig. 1a marked), which were identified mainly as Nb(C, N) by electron diffraction patterns. The sprayed water cooling steel microstructure is shown in Fig. 1b. It can be observed acicular ferrite type and bainite with an average grain size of about 10–15 μm. From TEM observations performed in these specimens, it was detected the presence of fine particles localized at the acicular ferrite grain boundaries (showed in insert of Fig. 1b marked). They were identified by means of electron diffraction patterns as TiN, Nb(C, N) and Mo_2C [15]. The microstructure of the water quenched specimen showed in Fig. 1c consisted of a combination of acicular ferrite, martensite and very few patches of bainite. From TEM images fine precipitates were observed in the martensite regions, which were identified by electron diffraction patterns as Nb(C, N) [15]. These precipitates showed an average size of 10 nm as observed in the insert in Fig. 1c marked. In the present work we could not clearly identify the presence of reverted austenite in the martensite matrix. It has reported that the presence of austenite in quenched steels not only improves its ductility and toughness but also has a higher ability to retard crack growth [5]. And, as reported by Zhao et al. [13] the presence of carbonitrides such as the ones found here will affect the mobility of dislocations, and thus, the transport of hydrogen, since dislocations can be pinned by the dispersed carbonitrides. The distribution of these particles was different for each one of the microstructures here, so this will affect the hydrogen effect on each steel with a different thermomechanical treatment.

The mechanical properties of these steels were performed in order to establish the influence of the different microstructures obtained from the heat treatments was shown in Table 1. From these results clearly the presence of acicular ferrite, martensite and bainite (steel 2F and 2A) raises the mechanical properties.

3.2. Polarization curves

Fig. 2 shows the effect of the temperature on the polarization curves for the three specimens. It can be seen that, for steel 2A, Fig. 2a, the curves did not show an active-passive behavior but only anodic dissolution, and the free corrosion potential value, E_{corr}, practically was not affected by the temperature, lying around −100 mV_{SCE} regardless the temperature. The anodic current density, however, increased as the temperature increased up to 70 °C, but it decreased with a further increase in the temperature up to 90 °C. Some instabilities can be seen in the anodic branch for the curve at 25 °C, which can be due to a disruption of the film formed by the corrosion products. It has been reported that the corrosion process of iron and/or steel in H_2S containing solutions generally is accompanied by the formation of iron sulfide films on the metal surface [23,24] which are porous, non-protective, and this is the reason why a passive region is not found on the polarization curve. Polarization curve for specimen 1T, Fig. 2b, was very similar to that shown by specimen 2A, and this may be

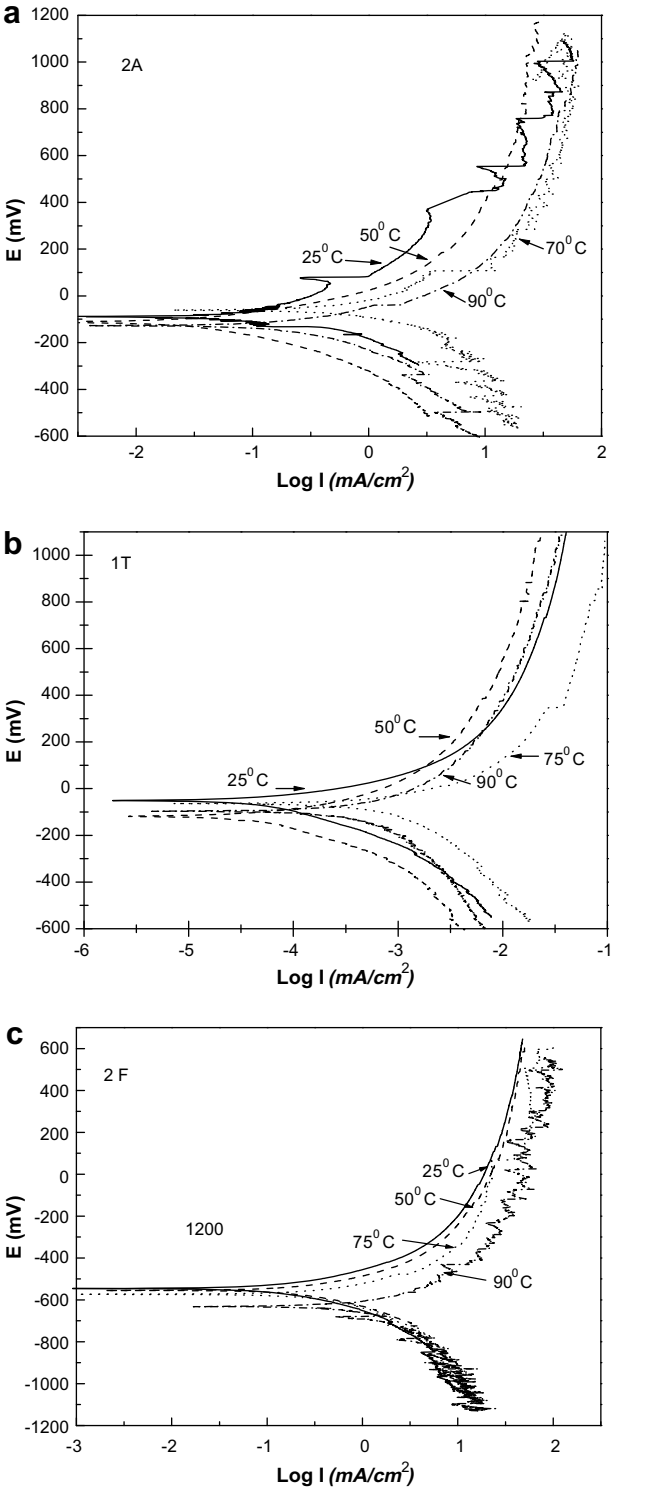

Fig. 2. Effect of temperature on the polarization curves for steel: (a) 2A, (b) 1T and (c) 2F.

because the former has a ferritic microstructure, whereas the later has a ferritic + bainitic microstructure. This time, the E_{corr} values lied between −50 and −150 mV_{SCE} with a tendency towards more active values as the temperature increased, and this time no instabilities were observed in the anodic branch. Polarization curves for the specimen with a martensitic microstructure, specimen 2F, showed E_{corr} values more active than those obtained for steels 1T and 2A, between −550 and −650 mV_{SCE}, with a tendency towards

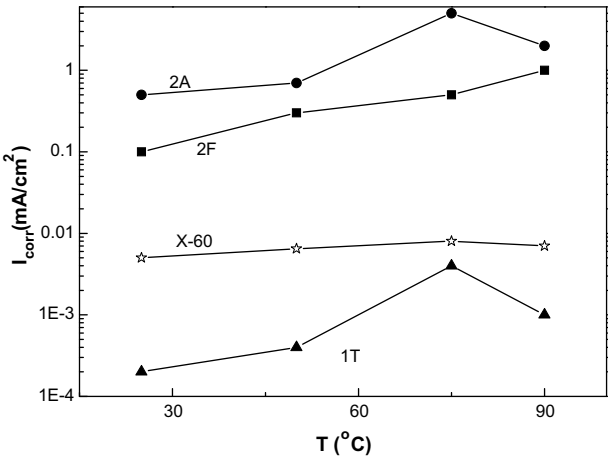

Fig. 3. Effect of temperature on the I_{corr} value for steels 2A, 2F and 1T.

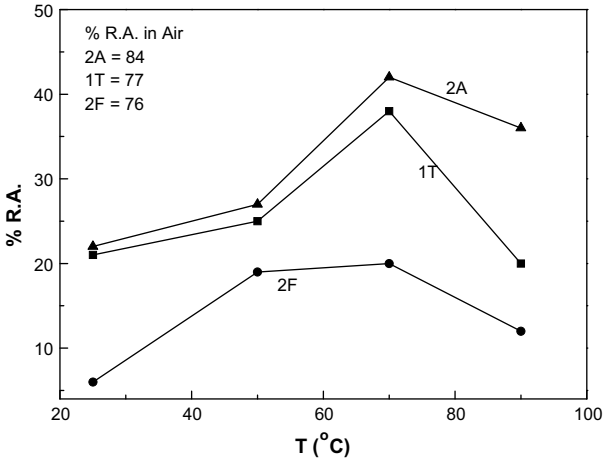

Fig. 4. Effect of temperature on the percentage reduction in area value for steels 2A, 2F and 1T.

more active values as the temperature increased, Fig. 1c. The anodic current density always increased as the temperature was increased this time, and the instabilities in the anodic branch due to film disruption were observed at 90 °C. Fig. 3 shows the effect of temperature in the corrosion current density value, I_{corr} for the three specimens. For materials 1T and 2A, this figure shows that the I_{corr} value increased with the temperature up to 70 °C but it decreases at 90 °C, whereas this value always increased with an increase in the temperature for specimen 2F. The specimen with the lowest I_{corr} value was steel 1T, whereas material 2A had the highest I_{corr} value, almost 4 orders of magnitude. The I_{corr} value for specimen 2F was close, but lower, to that obtained for material 2A. By comparing these results with those shown by a typical pipeline steel such as API X-60 steel, we can see that the steel which had lower corrosion rates was 1T for nearly one order of magnitude, so, this fact encouraged us to carry on with this work.

3.3. SSRT tests

Fig. 4 shows the effect of temperature on the susceptibility towards SSC as measured by the percentage reduction in area, %R.A., where it can be seen that the most susceptible material towards SSC was the martensitic one, i.e. 2F, whereas steels 2A, the ferritic one, and 1T, ferritic + bainitic, were susceptible only at 25 °C. In all cases, regardless the microstructure, there was a tendency to recover their ductility as the temperature increased up to 70 °C, but they lost the ductility once again at 90 °C. Working with a similar pipeline steel, Carneiro et al. [8] carried out similar thermo-mechanical treatments: rolling from 860 °C to 760 °C; after this, the steel was normalized at 900 °C, and then water quenched and tempered at 640 °C during 60 min. Microstructures exhibited by the rolled specimen was mainly ferrite(deformed) + pearlite, whereas for normalized steel it consisted of polygonal ferrite + pearlite + austenite/martensite. Finally, the quenched and tempered steel consisted of homogeneous martensite. The refined homogeneous quenched and tempered martensite improved the SCC resistance, whereas the rolled and normalized microstructures showed greater susceptibility to SCC. In our case, untempered martensite was the most susceptible to SCC for reasons given bellow. Fracture surfaces of specimens 2A, 2F and 1T are shown on Figs.

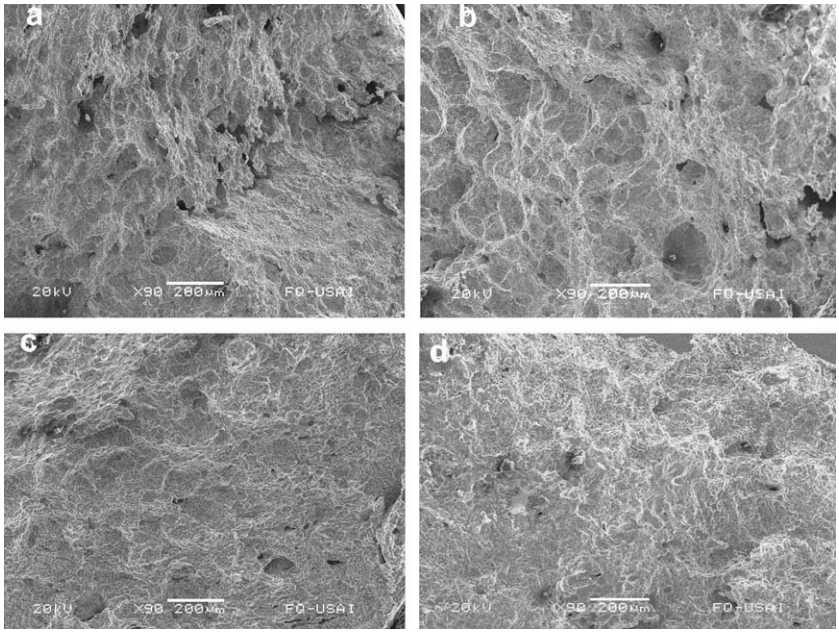

Fig. 5. Micrographs of the fracture surfaces for specimen 2A strained at: (a) 25, (b) 50, (c) 70 and (d) 90 °C.

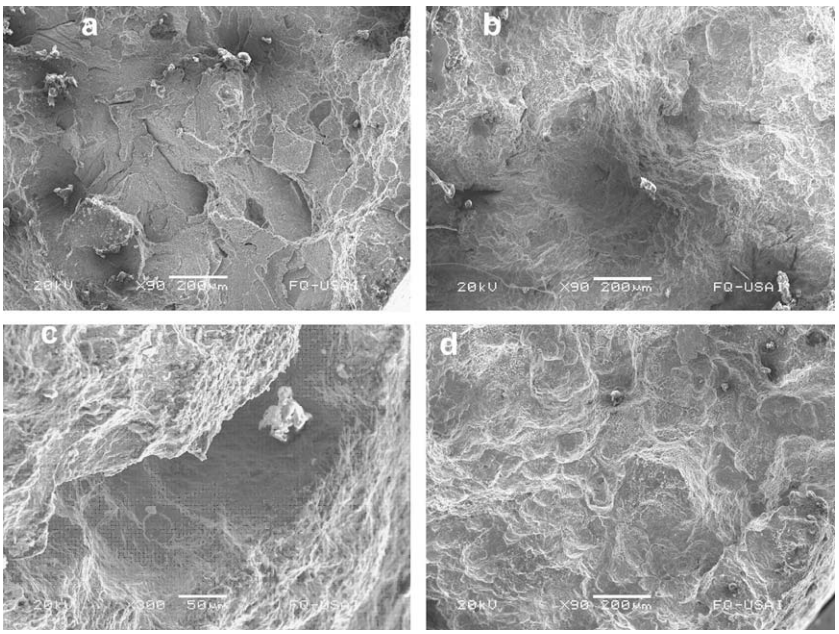

Fig. 6. Micrographs of the fracture surfaces for specimen 2F strained at: (a) 25, (b) 50, (c) 70 and (d) 90 °C.

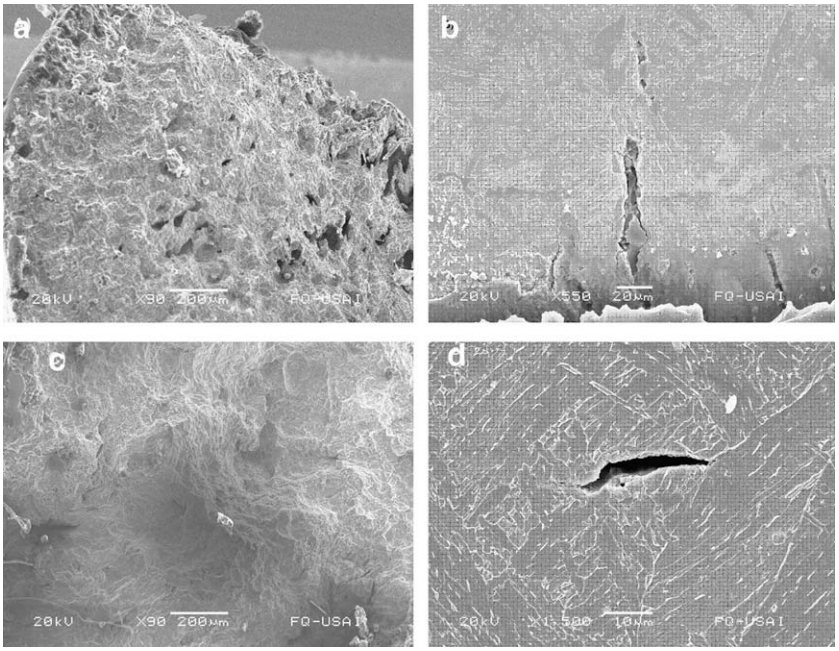

Fig. 7. Micrographs of the fracture surfaces for specimen 1T strained at: (a) and (b) 70 °C, and (c) and (d) 50 °C.

5–7 respectively. Generally, all the specimens, with high susceptibility towards SSC, showed brittle type of fracture, with transgranular cracks, quasicleavage features**,** typical of hydrogen embrittlement type of failure, and, in most of cases, with clear evidence of anodic dissolution taking place on the surface, which was more evident as the temperature increased.

3.4. Hydrogen permeation measurements

Fig. 8 shows a typical hydrogen permeation current density transient at 25 and 50 °C for specimen 2F, which shows that it increases slowly with time until it reaches a maximum value, and then it decreases, probably due to the formation of an iron sulfide film. When the temperature is raised up to 50 °C, the hydrogen permeation current density increases once again until a maximum value, and then it decreases once again. Fig. 9 shows the effect of the temperature on the number of hydrogen atoms at the entrance surface, C_0, for the three steels. Generally speaking, C_0 increases as the temperature increases, but this increase is more pronounced for steel 1T than for steels 2F and 2A. The highest C_0 values were obtained for the 1T, whereas the lowest C_0 values was obtained for steels 2F around one order of magnitude lower than that for steel 1T. On the other hand, the effect of the temperature on the effective hydrogen diffusivity value, D_{eff}, Fig. 10, shows that it in-

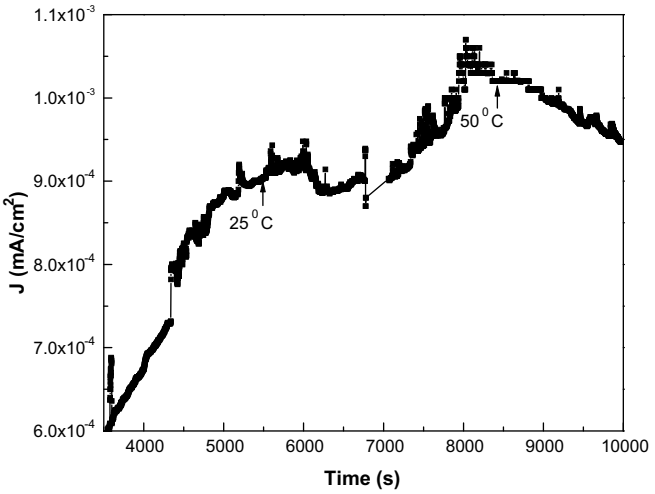

Fig. 8. Typical hydrogen permeation transients at 25 and 50 °C.

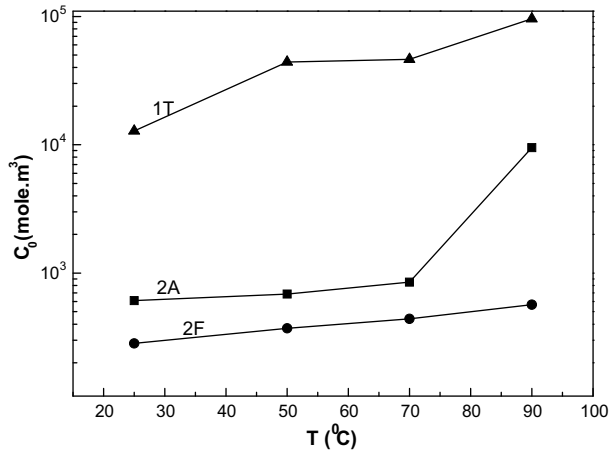

Fig. 9. Effect of temperature on the C_0 value for steels 2A, 2F and 1T.

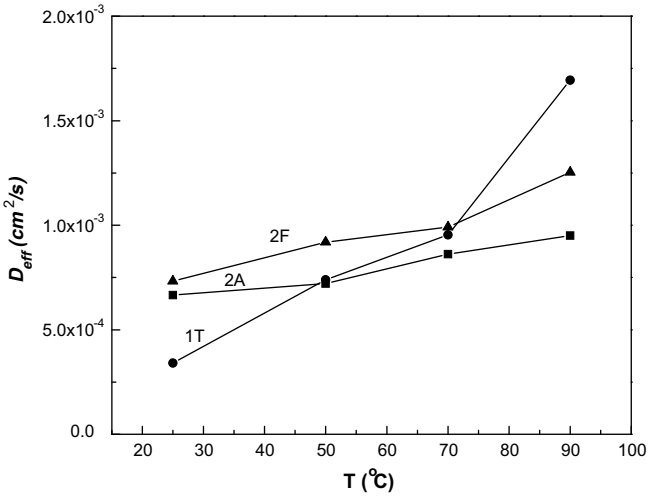

Fig. 10. Effect of temperature on the D_{eff} value for steels 2A, 2F and 1T.

creases as the temperature increases, obtaining the lowest value for material 1T and the highest for material 2F.

Fig. 4 shows that steel 2F showed the highest susceptibility to fail by SSC, and that this susceptibility decreased as the temperature increased. Conversely, Fig. 8 shows that this steel had the lowest number of hydrogen atoms at the entrance surface value, C_0, but the second highest corrosion current density values, I_{corr}, Fig. 3, and these values increased with temperature. On the other hand, steel 1T showed o much lower susceptibility to fail by SSC, Fig. 4, but it had the highest number of hydrogen atoms at the entrance surface value, C_0, Fig. 9, and the lowest I_{corr} value, Fig. 3. It is normally accepted that the SSC phenomenon is dominated by a hydrogen embrittlement mechanism [6–13]. These results seem to confirm this hypothesis: a material with a high corrosion rate (steel 2F) is the most susceptible to fail by SSC because hydrogen is produced as given by the following reactions:

Anodic reaction:

$$Fe \rightarrow Fe^{2+} + 2e^{-} \quad (5)$$

Cathodic reaction:

$$H_2S_{(aq)} + 2e^{-} \rightarrow S^{2-} + H_2 \quad (6)$$

Overall reaction:

$$Fe + H_2S_{(aq)} \rightarrow FeS + H_2 \quad (7)$$

Thus, the role of the anodic dissolution is to provide hydrogen atoms. Thus, a mechanism based on hydrogen absorption and embrittlement by the steel where anodic dissolution does not play the most important role seems to explain the cracking mechanism of pipeline steels in H_2S-containing solutions. The requirements for SSC based on the HE mechanism include a susceptible microstructure, a threshold level of hydrogen to induce cracking, and an applied or residual stress [27]. It can be assumed that the failed round tensile bars used in the present study expose every weld microstructure directly to the test solution. In this study, environmental factors which enhanced hydrogen uptake by the steels did also enhance the SSC susceptibility in all cases, and it did enhance the corrosion rate. Thus, the tensile tests showed that these steels are highly susceptible to SCC, especially at 25 °C, since in air the failure was completely ductile, whereas in the testing solution the fracture mode was very brittle, with very small percentage reduction in area values, and there were a big number of cracks induced by the solution. Since the SSC susceptibility, increases with the corrosion rate, and with the hydrogen uptake by the steel, which may indicate that in addition to the anodic dissolution mechanism, there may be a hydrogen embrittlement component in the failures observed in this study. This is so because, although the hydrogen uptake by the steel increases with temperature, hydrogen atoms move faster as the temperature increases also, which may indicate that it leaves the steel. Thus, it seems that the most likely mechanism in the SSC susceptibility of high strength microalloyed pipeline steels is hydrogen embrittlement assisted by anodic dissolution, at least with the present microstructure.

On the other hand, Fig. 9 shows that the number of hydrogen atoms at the entrance surface value, C_0, was higher for steel 1T than that for steel 2F as established above. This can be explained with the fact the hydrogen diffusivity was higher for steel 2F than for steel 1T, Fig. 10. It can be seen that the D_{eff} values are in the order between 10^{-4} to 10^{-3} cm^2/s, whereas a diffusional process in aqueous solution has D_{eff} values around 10^{-5} cm^2/s, not so far from our results. When the temperature increases, the D_{eff} value increases also, so the steel can be degassed more easily and the steel can recover its ductility, as observed in Fig. 4, where it can be seen that the ductility, as measured in the percentage reduction in area, increases as the temperature increases.

The fact that the quenched steel was most susceptible to SCC is due to that the martensite is a highly stressed microstructure because of the excess carbon trapped interstitially [18]. Hence, it is assumed that grain boundary carbon segregation coupled with severe internal stresses will render grain boundaries susceptible to stress corrosion crack propagation. The difference in hydrogen permeation properties is related with differences in microstructure. Lattice defects, such as dislocations, grain boundaries and interfaces between precipitates and matrix might trap substantial hydrogen decreasing the effective hydrogen diffusivity. According to their binding energy hydrogen traps are classified as reversible and irreversible [25]. Irreversible traps are responsible for a greater decrease in the effective diffusivity than reversible traps [26] and, depending upon chemical microstructure and heat treatment, metals will present nanometer sized (fine-coarse) carbides inside the metal matrix and at grain boundaries like those shown on Fig. 1. The presence of reverted austenite with a greater number of fine carbides homogenously distributed within martensite laths and in some retained austenite zones resulted in changing the nature of trapping sites for the water quenched steel, i.e. 2F. Unlike this, cooling with forced nitrogen gas, steel 2A, may have lower density of reversible and increased the irreversible trapping sites. Fig. 1a shows that steel 2A has a high population of bainite inclusions at grain boundaries, whereas steel 2F presents carbides mainly within grain boundaries and a few of them in the grain boundaries. Thus, bainite and associated precipitates could increment the hydrogen irreversible traps, explaining the lower D_{eff} value than that obtained for steel 2F, Fig. 10. On the other hand, sprayed water cooled steel, 1T, showed a bainitic microstructure along with ferrite, Fig. 1b, with larger carbides than those found in steel 2A, finely distributed along grain boundaries, with a lower dislocation density than the other two steels, and achieved lower D_{eff} values. Heat treatments as those given to steels 1T and 2A can change the nature and number of trapping sites, and, thus, change the transport of hydrogen towards the crack tip.

4. Conclusions

Studies of the effect of the microstructure and temperature on the sulphide stress cracking, SSC, susceptibility of a high strength microalloyed pipeline steel has been carried out. The most important results are:

(a) The corrosion rate, taken as I_{corr}, increased with an increase in the temperature from 25 to 90 °C, regardless of the microstructure, being highest for a ferritic steel, whereas the lowest I_{corr} value was for a martensitic steel.
(b) The amount of hydrogen uptake for the steels increased with increasing temperature, being highest for a martensitic steel, and the lowest was for a ferritic steel.
(c) The most susceptible steel was the martensitic, whereas ferritic and ferritic + bainitic steels were highly susceptible at 25 °C. The SSC susceptibility decreased with increasing the temperature for all microstructures from 25 to 70 °C but then it decreased with a further increase up to 90 °C.
(d) The most likely mechanism for the cracking susceptibility a high strength microalloyed pipeline steel in H_2S solutions seems to be hydrogen embrittlement, whereas anodic dissolution seems to play a secondary role in the cracking mechanism.

References

[1] B.J. Berkowitz, F.H. Heubaum, Corrosion 40 (5) (1984) 240–245.
[2] A.T. Yokobori Jr., T. Nemoto, K. Satoh, T. Yamada, Eng. Fract. Mech. 55 (1) (1996) 47–60.
[3] J.H. Chuang, L.W. Tsay, C. Chen, Int. J. Fatigue 20 (7) (1998) 531–536.
[4] T.L. Chang, L.W. Tsay, C. Chen, Mater. Sci. Eng. A 316 (1/2) (2001) 153–160.
[5] L.W. Tsay, W.C. Lee, R.K. Shiue, J.K. Wu, Corros. Sci. 44 (9) (2002) 2101–2118.
[6] L.W. Tsay, M.Y. Chi, Y.F. Wu, J.K. Wu, D.Y. Lin, Corros. Sci. 48 (8) (2006) 1926–1938.
[7] D. Hardie, E.A. Charles, A.H. Lopez, Corros. Sci. 48 (12) (2006) 4378–4385.
[8] Rogerio Augusto Carneiro, Rajindra Clement Ratnapuli, Vanessa de Freitas Cunha Lins, Mater. Sci. Eng. A 357 (2003) 104–110.
[9] Chengqiang Ren, Daoxin Liu, Zhenquan Bai, Tiehu Li, Mater. Chem. Phys. 93 (2005) 305–309.
[10] Her-Hsiung Huang, Ju-Tung Lee, Wen-Ta Tsai, Mater. Chem. Phys. 58 (1999) 177–181.
[11] Y.Y. Chen, Y.M. Liou, H.C. Shih, Mater. Sci. Eng. A 407 (2005) 114–126.
[12] L.W. Tsay, M.Y. Chu, H.R. Chen, C. Chen, Mater. Sci. Eng. A 416 (2006) 155–160.
[13] Ming-Chun Zhao, Yi-Yin Shan, Fu Ren Xiao, Ke Yang, Yu Hai Li, Mater. Lett. 57 (2002) 141–145.
[14] I. Takechi, J. Fujino, A. Yamamoto, S. Okaguchi, The prospects for high-grade steel pipes for gas pipelines, Pipes Pipelines Int. (2003) 33–43.
[15] R. Mendoza, J. Camacho, G. Lugo, C. López, L. Herrera, C. Gonzalez, J.A. Juárez-Islas, Structure of a low carbon Al-killed/Ti added steel, Iron Steel Int. J. 37 (2) (1997) 176–180.
[16] R. Mendoza, J. Huante, M. Alanis, C. Gonzalez, J.A. Juarez-Islas, Ironmak. Steelmak. 26 (3) (1999) 205–209.
[17] S. de Meester, Iron Steel Int. J. 37 (6) (1997) 537–551.
[18] S. Lee, D. Kwon, Y.K. Lee, O. Kwon, Metall. Mater. Trans. A 36 (1995) 1093–1100.
[19] Y. Shunfa, C. Gouping, C. Meifang, in: HSLA Steel Metallurgy and Applications, International Conference on H.S.L.A. Steels, ASM, Metals Park, OH, 1986, pp. 213–218.
[20] K. Hulka, F. Heisterkamp, I.I. Frantov, in: R. Denys (Ed.), An Economic Approach to Pipe Steels with High Toughness and Good Weldability, Pipeline Technology Conference Proceedings, Antwerpen, Belgium, 1990, pp. 45–65.
[21] A.J. De Ardo, Int. Mater. Rev. 48 (6) (2003) 371–402.
[22] M.A. Devanathan, Z. Stachurski, Proc. Roy. Soc. (London) 270 (1962) 90–102.
[23] E. Sosa, R. Cabrera-Sierra, E. Marina, M.E. Rincon, M.T. Oropeza, I. Gonzalez, Electrochim. Acta 47 (2002) 1197.
[24] H. Ashassi-Sorkhabi, S.A. Nobavi-Amri, Electrochim. Acta 47 (2002) 2239.
[25] R. Gibala, D.S. DeMiglio, in: I.M. Bernstein, A.W. Thomson (Eds.), Proceedings of the Third International Conference on Hydrogen Effects in Metals, AIME, 1980, pp. 113–119.
[26] G.M. Pressouyre, I.M. Bernstein, Metall. Trans. 9A (11) (1978) 1571–1580.
[27] A.J. Griffiths, A. Thurnbull, Corrosion 53 (9) (1997) 700–711.